BROOKHAVEN
NATIONAL LABORATORY

BNL-75556-2006-CP

Two-Phase Flow Studies in Nuclear Power Plant Primary Circuits Using the Three-Dimensional Thermal-Hydraulic Code BAGIRA

S. D. Kalinichenko, A. E. Kroshilin, V. E. Kroshilin, A. V. Smirnov
All-Russian Research Institute for Nuclear Power Plant Operations (VNIIAES)
25 Ferganskaya St., 109507 Moscow, Russia

P. Kohut
Brookhaven National Laboratory
Bldg. 475, Upton, NY 11973, USA
Tel: 631-344-4982, Fax: 631-344-7650, Email: Kohut@bnl.gov

Proceedings of ICAPP '06
Reno, Nevada
June 4-8, 2006

April 2006

Energy Sciences & Technology Department

Brookhaven National Laboratory
P.O. Box 5000
Upton, NY 11973-5000
www.bnl.gov

DISCLAIMER

Proceedings of ICAPP '06
Reno, NV USA, June 4-8, 2006
Paper 6066

Two-Phase Flow Studies in Nuclear Power Plant Primary Circuits Using the Three-Dimensional Thermal-Hydraulic Code BAGIRA

S. D. Kalinichenko, A. E. Kroshilin, V. E. Kroshilin, A. V. Smirnov
All-Russian Research Institute for Nuclear Power Plant Operations (VNIIAES)
25 Ferganskaya St., 109507 Moscow, Russia

P. Kohut
Brookhaven National Laboratory
Bldg. 475 Upton, NY 11973, USA
Tel: 631-344-4982, Fax: 631-344-7650, Email: kohut@bnl.gov

Abstract – *in this paper we present recent results of the application of the thermal-hydraulic code BAGIRA to the analysis of complex two-phase flows in nuclear power plants primary loops. In particular, we performed benchmark numerical simulation of an integral LOCA experiment performed on a test facility modeling the primary circuit of VVER-1000. In addition, we have also analyzed the flow patterns in the VVER-1000 steam generator vessel for stationary and transient operation regimes. For both of these experiments we have compared the numerical results with measured data. Finally, we demonstrate the capabilities of BAGIRA by modeling a hypothetical severe accident for a VVER-1000 type nuclear reactor. The numerical analysis, which modeled all stages of the hypothetical severe accident up to the complete ablation of the reactor cavity bottom, shows the importance of multi-dimensional flow effects.*

I. INTRODUCTION

The three-dimensional thermal-hydraulic best-estimate code BAGIRA[1, 2] was developed at VNIIAES within the last decade to enable the modeling of a wide range of two-phase flow phenomena in Nuclear Power Plant (NPP) primary loops, both for boiling and pressurized water reactors. The main purpose of the code is to allow comprehensive safety analysis of NPPs.

The physics model was developed for general multi-phase mixture flow with the following features. The two-phase reactor coolant is a general mixture of liquid and gas phases with the gas phases being a mixture of vapor and non-condensed gas. Each phase (liquid or gaseous) is characterized by its own velocity and temperature. In the general case, phase temperatures may differ from the saturation temperature. Non-stationary, multi-dimensional flows are considered when necessary.

The mathematical model implemented in the BAGIRA code includes: mass balance equations of mixture, liquid, and non-condensed gas, mixture internal energy balance, gas phase enthalpy balance, and momentum equation(s). Two versions of the code are available; the basic version is based on the drift model using the single momentum equation for the mixture, supplemented with a correlation for finding the relative phase velocity. An optional model is also available involving two separate momentum equations for the liquid and gas phases respectively.

The code was developed from the beginning with a three-dimensional numerical scheme by approximating the main equations of hydrodynamics without any additional physical assumptions or simplifications. All physical parameters have full spatial dependencies i.e., depend on three spatial coordinates, while vector quantities are considered with full three-components. The computational efficiency of the numerical scheme allows most analysis to be performed in real-time, without loss of accuracy.

Well-known and highly accurate empirical correlations are used for the inter-phase and phase-wall interaction as well as description of heat exchange.

BAGIRA has been carefully verified using experimental data from various measurements:

- Laboratory experiments modeling specific physical phenomena;
- Experiments on integral test facilities;
- Experiments performed on operating NPPs;

- Comparison with the results of obtained by other best-estimate thermal-hydraulic codes.

The full list of experiments used for the verification of the code is given in a previous paper[3]. More detailed information concerning the verification of BAGIRA can also be found in another recent papers.[4, 5]

In this paper we focus on the application of BAGIRA to the analysis of complex phenomena, which takes place in the primary coolant circuits of NPPs (or in integral facilities modeling reactors) in transient and accident operating regimes. Special attention was paid to model and analyze cases where multi-dimensional effects play essential roles.

The paper is organized as follows. In Sec. II below, we present new results obtained after modeling a small-break primary circuit LOCA experiment that was performed on the PSB-VVER integral test facility. This experiment is characterized by a variety of complex and interrelated physical phenomena, which play a significant role in NPP safety. Sec. III presents the application of BAGIRA for two-dimensional analysis of two-phase flows in a VVER-1000 steam generator (SG) vessel. In Sec. IV we perform numerical simulation of a hypothetical severe accident for a typical VVER-1000 NPP design initiated by a large break of one of the primary loops. The three-dimensional nodalization of the reactor vessel allows detailed study of the coolant parameter distributions across the core region.

II. NUMERICAL ANALYSIS; PSB-VVER INTEGRAL TEST FACILITY, COLD LEG SMALL BREAK, 3% LEAK

The PSB-VVER facility constructed in Electrogorsk Research & Engineering Center is the most recent Russian thermal-hydraulic test unit modeling the primary circuit of a typical VVER-1000 reactor. PSB-VVER has four circulation loops and is scaled to 1:300 in volume and power (at maximum power level), and 1:1 in height to a VVER-1000 reactor. The main elements of the PSB-VVER test facility are shown in Fig. 1. The facility is also equipped with a number of auxiliary systems, which allow studying various methods in controlling accident events. The most important auxiliary system is the emergency core coolant system (ECCS) consisting of three sub-systems: four passive hydro-accumulators, and a coupled high and low-pressure injection systems.

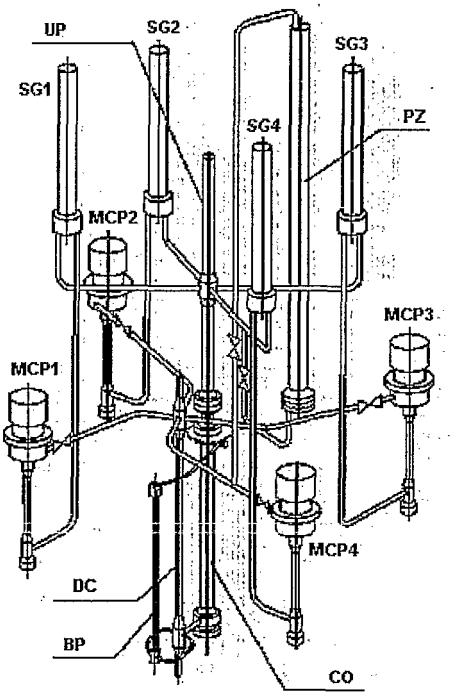

Fig. 1. General view of PSB-VVER integral test facility: CO – core model, MCP – main coolant pump, BP – bypass, PZ – pressurizer, DC – downcomer, SG – steam generator, UP – upper plenum

The reactor core is simulated by 168 electrically heated fuel rods with a maximal heating power of 10 MW. The fuel elements are separated by 15 spacer grids.

In the following we present new analytical results of the recent small-break experiment "Cold leg break, 3% leak" performed on the PSB-VVER integral test facility.

In the experiment, the initial, steady-state of coolant had the following characteristics (listed in Table I).

TABLE I

Initial conditions of experiment in PSB-VVER test facility

Parameter	Value
Upper plenum pressure	15.4 MPa
Inlet/outlet coolant temperature at the core region	281.5/317°C
Core model heating power	1.5 MW
Bypass heating power	15 kW
Secondary side pressure	6.9 MPa
Pressure in accumulators	4.06 MPa

Note that in this experiment the heating power of the fuel rod assembly was considerably lower (15%) than the scaled down maximum power.

The four SG's were joined to a common steam collector; while the two accumulators were connected to the downcomer (the second pair of the accumulators joined to the upper plenum, but was not used in this experiment). The break unit was inserted into the cold leg of the No. 4 loop, between the main coolant pump (MCP) and downcomer inlet.

Since the pipe diameters are much less then their lengths, we used a one-dimensional nodalization scheme to model the experiment. Each primary loop, as well as each SG's, was modeled separately. The full primary and secondary circuit models contained 276 and 42 cells respectively.

A comparison of the calculated and experimental values for the most important thermal-hydraulic parameters is shown in Figs. 2 through 9.

The experiment is initiated at time t = 0 s by opening the break line. Simultaneously, the valves regulating the steam extraction from the SG's and the feed-water supply begin closing and the MCPs are shut down. The discharge of the large amount of coolant through the break leads to a rapid fall in the primary circuit pressure (Fig. 2). When the pressure reaches the value 13.7 MPa, the core and bypass heating power begins to reduce according to a preset ramp-down rate.

In the secondary circuit, the pressure initially increases due to the heat transferred from the primary circuit. However, the pressure increase is stopped by the steam dump system (quick-acting pressure reduction valves) having a set point for opening/closure at 7.5/7.0 MPa. Repeated activations and deactivations of the steam dump system results in a pressure oscillation in the secondary side (Fig. 3) between the time interval t = 0-250 s.

Due to the coolant discharge, the upper part of the primary circuit becomes gradually voided. This may be seen from the time dependent behavior of the pressure drop (Fig. 4). Since the characteristic values of the coolant flow rates are relatively small, the pressure drop is primarily determined by the volumetric water fraction in the core.

At about t = 480 s the upper part of the channel with the simulated fuel rod bundle is completely uncovered resulting in a core heat-up accompanied by an increase in the fuel rod cladding temperature (Fig. 5). When the clad temperature reaches the value of 500°C (at t = 625 s), the active low-pressure ECCS is activated for about 25 s (then it switched off). Coolant enters into the No. 1, 3, and 4 loops with a flow rate of 0.3 kg/s. Note that despite the water being injected by the active ECCS, the fuel rod cladding temperatures keeps increasing.

At t = 673 s the primary side pressure falls to 4 MPa corresponding to the passive ECCS activation condition. The two accumulators begin supplying cold water into the upper part of the downcomer. After the passive ECCS activation the water level in the reactor region starts increasing, as seen on Fig. 4. Nevertheless, the coolant entering the upper part of the core is evaporated into droplets by the hot fuel rods and the clad temperature remains much greater than the saturation temperature. Its maximum value is reached at about t = 830 s (both in the experiment and in the calculation) and equals 692°C in the experiment and 661°C in the calculation.

As seen from Figs. 4 and 5, the passive ECCS is able to compensate (over a rather long time interval) the water discharge through the break. The core gradually fills up with water, while the fuel rod clad temperatures decreases.

Soon after the passive ECCS is initiated an interesting asymmetric phenomenon can be observed between the four loops. Hot vapor produced in the core region rises to the upper plenum and then condenses into the loops. However, liquid cold water injected by the active ECCS into loops Nos. 1, 3, and 4 forms a liquid "plug" preventing natural circulation of coolant (vapor). In loop No. 2, without direct ECCS water injection, the cold liquid "plug" is smaller, and is pushed from the loop to the downcomer by the stream of vapor from the core region. As a consequence natural circulation is restored in loop No. 2, while in loops Nos. 1, 3, and 4 the coolant remains stagnant. This can clearly be seen in Figs. 6-9: hot vapor from the core region enters loop No. 2, resulting in a peak of coolant temperature near t = 1000 s (Fig. 7), while in the other loops only small coolant temperature oscillations are observed (Figs. 6, 8, and 9).

The pressure drop oscillations, starting from t = 1200 s (see Fig. 4), can be explained by the changes in vapor generation intensity in the upper part of the core. The water level increases in the core region due to the injected coolant from the accumulators, resulting in an increase in vapor generation intensity. At the same time, the primary circuit pressure becomes almost stable reducing the flow rate from the accumulators, which depend on the pressure difference between the primary circuit and the accumulators. Coolant in the core gradually boils away, while the intensity of the vapor generation decreases and the primary circuit pressure starts to fall again increasing the accumulator injection flow rate. These processes repeat many times, leading to the pressure drop oscillations observed both in the experiment and calculations. Periodical core dry-out and reflood processes result in the fuel element clad temperature oscillations, starting from t = 2100 s (Fig. 5). Similar oscillations, but with lower magnitude, are also seen for the coolant temperatures in the primary loops (Figs. 6-9).

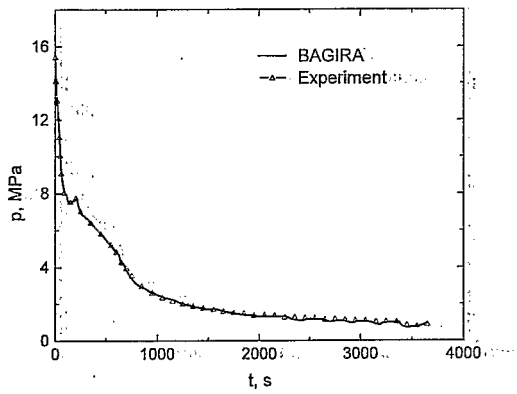

Fig. 2. Pressure in primary circuit

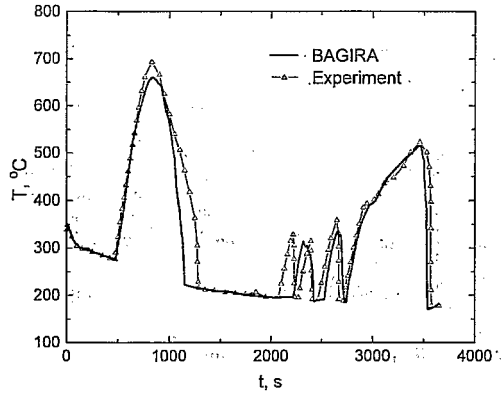

Fig. 5. Fuel rod clad temperature

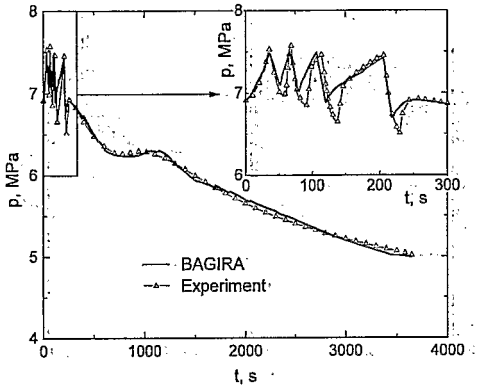

Fig. 3. Pressure in secondary circuit

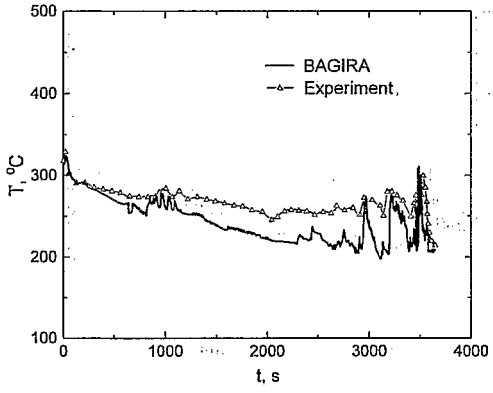

Fig. 6. Coolant temperature in loop No. 1

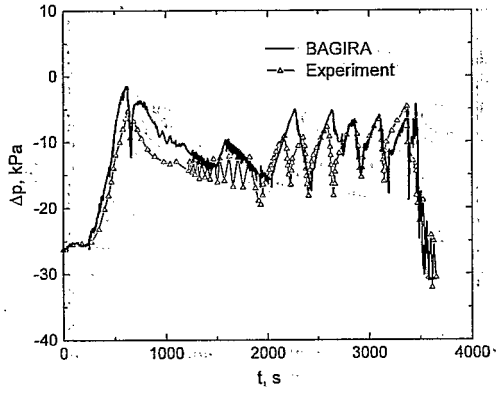

Fig. 4. Pressure drop in downcomer

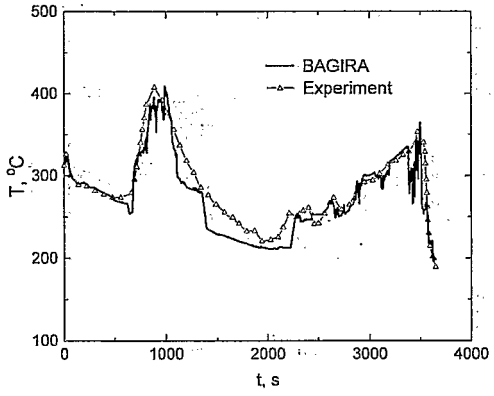

Fig. 7. Coolant temperature in loop No. 2

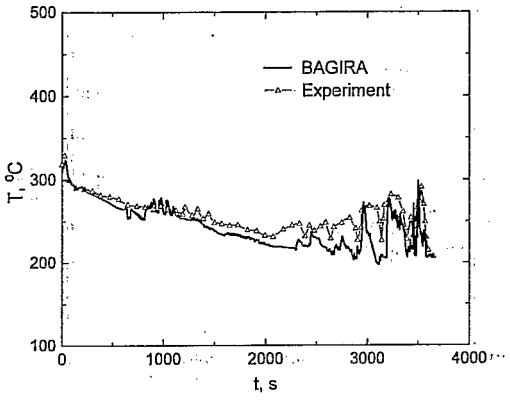

Fig. 8. Coolant temperature in loop No. 3

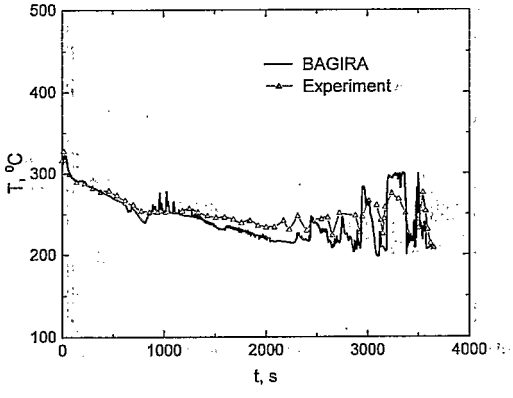

Fig. 9. Coolant temperature in loop No. 4

At about t = 3300 s the water supply in the accumulators is exhausted and the core region dries-out leading to a sharp increase in the fuel element clad temperature. When the temperature reaches the preset value of 500°C, the active low pressure ECCS is again activated, but now it keeps injecting coolant till the end of the experiment at t = 3650 s. The active ECCS coolant flow rate is sufficient not only in compensating the coolant loss through the leak, but also ensuring the complete refill of the core region with water.

The sequence of the main events observed in the experiment is listed in Table II, where the corresponding timings are also indicated, both for the experiment and calculation.

TABLE II

Main events during experiment on PSB-VVER test facility

Event	Time, s (Exp.)	Time, s (Calc.)
Break line opening	0	0
Start of coolant boiling-up in primary circuit	15	16
Start of core heating power reduction and pump shutdown (p<13.0 MPa)	18	19
Start of first core heating-up	474	479
First active low-pressure ECCS activation ($T_{fuel\ rod\ clad}$=500 °C)	629	628
Passive ECCS activation (p<4 MPa)	673	677
Maximal fuel rod clad temperature is reached	829	835
First core reflood completed	1290	1150
Start of second core heating-up	2060	2190
Water supply in accumulators is exhausted	3160	3192
Second active low-pressure ECCS activation ($T_{fuel\ rod\ clad}$=500 °C)	3368	3372
End of experiment	3650	3650

The comparison of calculated and experimental results shows that BAGIRA can successfully reproduce the most important processes observed in the experiment. The behaviors of both the primary and secondary circuit pressures are described very accurately. The timing of the core heat-up is also predicted very well including the value of the maximum fuel rod cladding temperature.

III. MODELING OF A HORIZONTAL VVER-1000 STEAM GENERATOR

Unfortunately, detailed verification of multi-dimensional multi-phase flow models is rather difficult due to lack of good quality experimental data. This especially true regarding the characteristics of multi-dimensional phenomena in NPP circuits, since these events are extremely difficult to model and can not be conducted in full-scale laboratory conditions. In light of these difficulties, special tests performed at actual NPPs, aimed at measuring multi-dimensional effects, are of great value. A good example of this type of experiment was performed at the Novovoronezh Unit No. 5 NPP, where the characteristics of two-phase coolant flow were investigated in a horizontal SG[6]. In the experiment, the volumetric water-vapor mixture velocity and void fraction were measured as a function of reactor power in the gap between the SG vessel and the "hot" side of the heat- exchanger tube bundle.

The SG vertical cross section is shown schematically in Fig. 10. The primary circuit coolant enters the cylindrical inlet header, then goes through the horizontal heat-

exchanger tube bundle and collects in the outlet header. Steam demand is balanced with the help of a perforated plate installed above the heat-exchanger tubes. Two vertical submerged shields are also placed between the SG vessel and the "hot" and "cold" parts of the tube bundle. Feed water enters through 16 inlet pipes entering the SG vessel between the perforated plate and heat-exchanger tubes. Steam moves through the separator and enters the steam collector. The design is based on the assumption that during normal operation the coolant moves down in the gap between the vessel and the submerged shield on the "hot" side of the bundle.

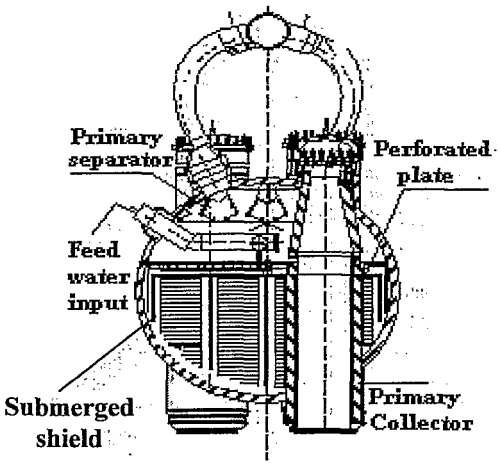

Fig. 10. SG vertical cross section

In Fig. 11 the simplified longitudinal (top view) and transversal SG cross sections near the region of the inlet ("hot") header are shown. Since the SG tube lengths are different, the coolant temperature distribution measured inside the tubes in the same transversal cross section is non-uniform. Indeed, the maximum coolant temperature is reached near the "hot" header (point A in Fig. 11a). Due to the heat transfer from primary to secondary circuit, the coolant temperature gradually decreases along each tube. This leads to a spatial variation in the temperature distribution, i.e., the coolant temperature at point B is less than that at point A, but larger than at point C (see Fig. 11a). The corresponding coolant temperature distribution in the primary circuit is shown in Fig. 11b with red being the highest and blue indicating "colder" temperatures. This spatial effect leads to a non-uniform thermal flux distribution from the primary to secondary circuit. Increasing thermal flux results in a decreasing secondary side coolant density that leads to an upward coolant flow in the SG vessel near the "hot" header and downward flow in the gap between the SG vessel and "hot" submerged shield. The resulting circulation pattern is shown in Fig. 11b (red arrows).

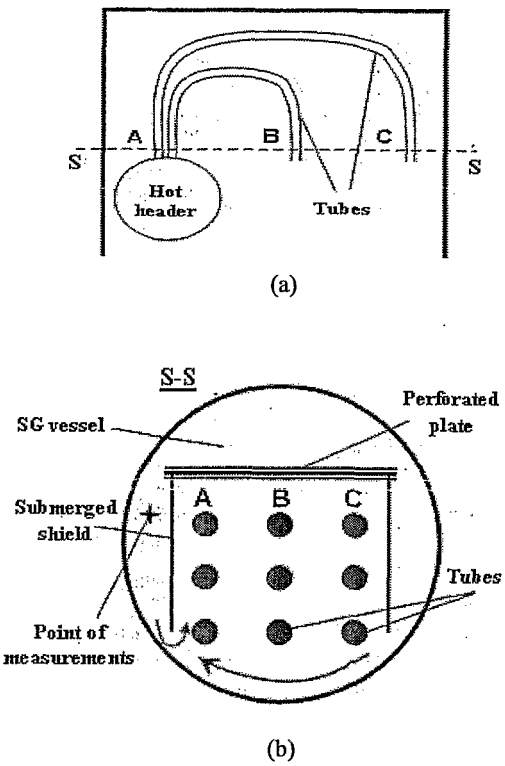

Fig. 11. Schematic layout of SG main elements: (a) Top view, and (b) cross section S-S (arrows show design circulation path)

However, the measurements revealed a quite different coolant flow pattern in the secondary circuit near the inlet header. In the gap, between the SG vessel and the submerged shield on the "hot" side, the coolant rises steadily. Under such conditions water flows from the gap into the space above the perforated plate that increases steam humidity and reduces its quality. This flow pattern can not be correctly described by one-dimensional calculations, requiring a multi-dimensional approach.

The SG length reasonably exceeds its width, and the longitudinal gradients of coolant parameters are much smaller than the transversal ones. For this reason the characteristic transversal flux velocities are greater than the longitudinal ones at least by an order of magnitude. Taking this into account, we used a model with a two-dimensional nodalization scheme, which allows the modeling of coolant flow in the SG cross section by neglecting the longitudinal flux. Specifically, we considered the cross section near the "hot" header due to the strong difference in the specific thermal flux at the heat-exchanger tube-bundle (thermal flux ratios at the "hot", "middle", and "cold" parts relate to each other as 4:2.5:1).

The SG nodalization scheme is shown in Fig. 12. It includes all important SG elements shown in Fig. 11b: the

"hot" (between the first and second layers, in X-direction) and "cold" (between the last and next-to-last layers, in X-direction) submerged shields, the perforated plate (between the 5th and 6th layers, in Z-direction), the "hot" (X = 2), "middle" (X = 4), "cold" (X = 6) parts of the tube-bundle, and the channels between the heat-exchanger tubes (X = 3, X = 5). Feed water is injected at layer Z = 5, and due to the special method of feed water injection, the specific feed water flow-rates in the 2nd and 3rd layers (X = 2, 3) are equal to each other, while the flow-rate in the 4th layer (X = 4) is half of the other two layers. The perforated plate was modeled by appropriately adjusting the flow area and the hydraulic resistance coefficients on the corresponding cell boundaries.

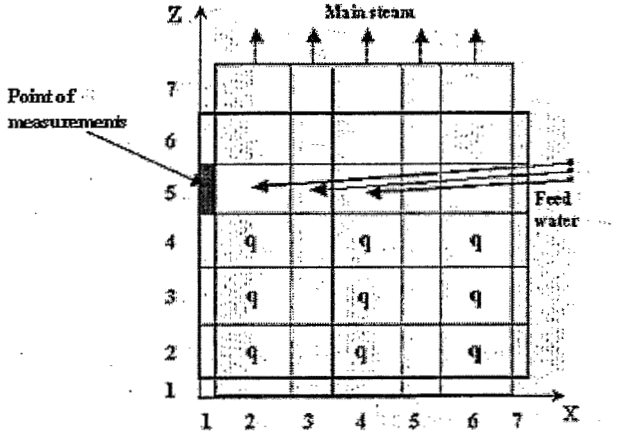

Fig. 12. SG nodalization scheme

The calculated water velocity and mixture volumetric velocity profiles are shown in Figs. 13 and 14, respectively, for rated SG operating conditions. The analysis predicts a global water circulation pattern in the whole SG cross section. In the "cold" sections, the coolant moves downward, while in the "hot" and middle sections the flow rises due to the reduced density of hot water. The coolant is rising in the gap between the SG vessel and the submerged shield, contradicting the SG design assumptions for the operating regime. The main reason for this phenomenon is the vapor generation in the gap region near the "hot" tube bundle as the vapor in all layers moves upwards. In general, the mixture volumetric velocity profile is analogous to the water velocity distribution with some specific differences. The vertical component of the water velocity near the perforated plate (both above and below) is close to zero, while the vertical component of the mixture volumetric velocity, in the same region, is quite significant at 0.5 m/s. We have also calculated the coolant flow parameters at reduced reactor power, which indicated that the main qualitative features of the flow pattern remains similar to the pattern seen at nominal power.

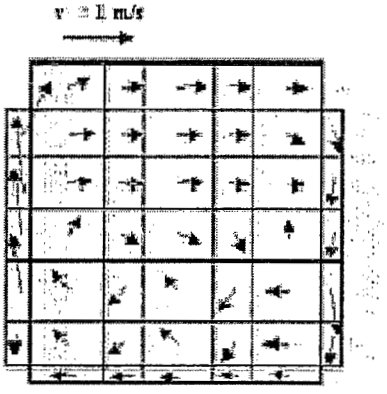

Fig. 13. Calculated water velocity profile

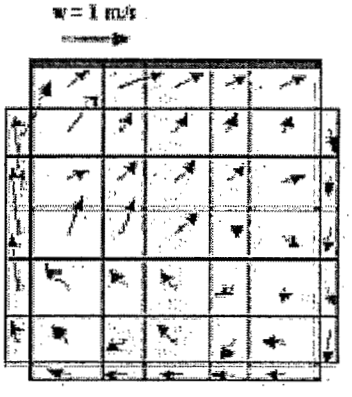

Fig. 14. Calculated mixture volumetric velocity profile

Figure 15a & b compares the dependencies on the relative reactor power of the calculated and measured parameters in the gap between the SG vessel and the "hot" submerged shield (corresponding to layer X = 1, Z = 5 in Fig. 12).

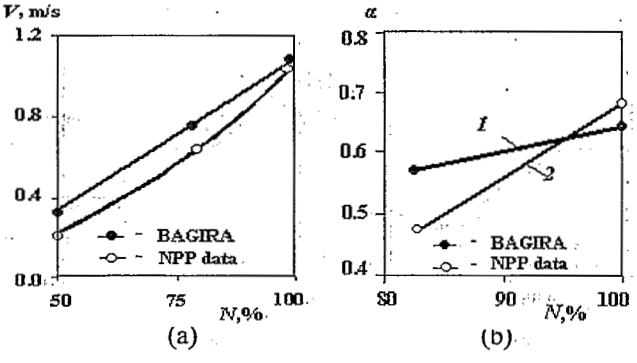

Fig. 15. Volumetric velocity (a) and void fraction (b) as a function of relative reactor power

Measured plant data, corresponding to the volumetric void fraction, α, in the central (X = 5) and "hot" (X = 3) channels, are listed in Table III together with the calculated values.

TABLE III

Comparison of measured and calculated void fraction values

Volumetric void fraction	BAGIRA	NPP data
Central channel region	0.41	0.28
"Hot" channel region	0.59	0.58

The calculated volumetric void fraction is in good agreement with the measurement in the "hot" channel while in the central channel the difference between is about 30%. However, the calculation was performed without specifically adjusting any of the free variable parameters (i.e. hydraulic resistance coefficients, turbulent mixing parameters, etc.), which could have been used to adjust the relative velocities of the coolant phases near the perforated plate to better match the experimental values. Considering this restriction, we conclude that the complex, nontrivial flow regime in the central channel reproduced the experimental data quite well.

To validate the above described SG model using dynamic transients, we also preformed a comparison of calculated and experimental data for a SG isolation test. This analytical study was done as part of the development of the full-scope simulator for the Kalinin NPP Unit No. 2 (VVER-1000), which used measured plant data for transient events including a SG isolation test. The simulator includes full three- and two-dimensional models for the reactor vessel and SG's, respectively.

The most important measured plant parameters together with the calculated results are shown in Figs. 16-18. In the plant test all SG isolation valves are closed and consequently the steam flow-rate from all SG's is reduced to zero. This leads to an increase in the pressure and water level in SG's at $t < 10$ s; since the feed water flow-rate remains constant. The maximum value of pressure in the main steam collector and SG vessels is practically the same, and equals about 7.25 MPa, in good agreement with the experimental observations. The increase in water level is clearly seen in the calculated curve in Fig. 18.

The experimental data does not seem to indicate a similar increase in the measured water level, which is probably due to the rather long periods between successive measurements. As the secondary side pressure increases, the coolant temperature also increases near the heat-exchange tube bundle due to saturation conditions. As a result, the coolant temperature difference between the primary and secondary sides of the SG's is reduced leading to a reduction of heat transfer from the primary circuit and increase in pressure at $0 < t < 15$ s. Due to the pressure increase the reactor emergency protection and scram systems are actuated to reduce reactor power decreasing the primary circuit pressure.

When the secondary circuit pressure exceeds a certain predetermined level, emergency steam removal systems are activated, sharply increasing the steam flow-rate from the SG's, while the water level falls. Finally all the parameters come to their stationary values.

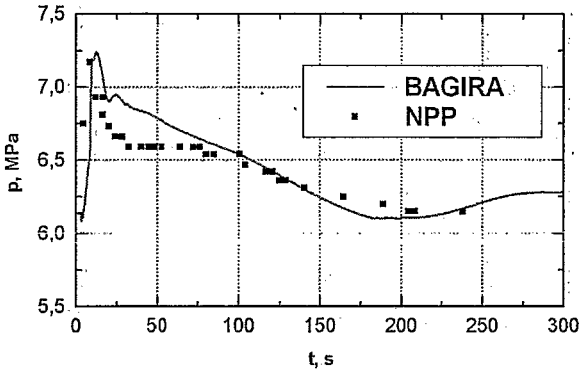

Fig. 16. Pressure in main steam collector

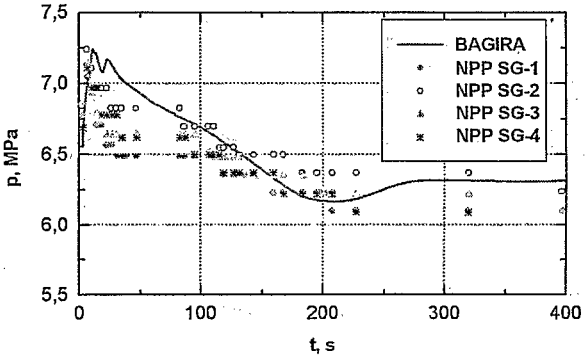

Fig. 17. Pressure in SG vessels

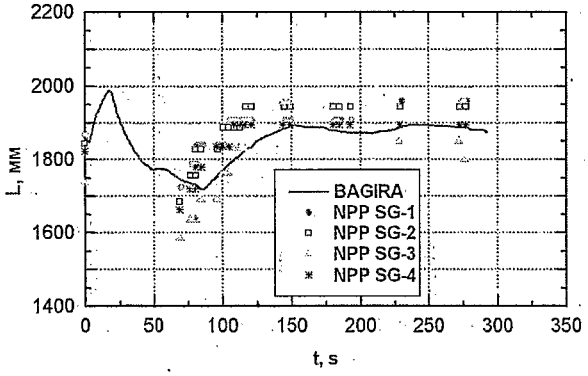

Fig. 18. Water level in SG vessels

The above results indicate that BAGIRA can adequately reproduce the complex phenomena observed in a SG isolation valve closure test.

The two-dimensional SG nodalization scheme used in our calculations has been primarily developed to be used in a full-scope plant simulator. In order to increase the computational details and accuracy, work is under way to develop a full three-dimensional SG nodalization scheme containing about 10^4 cells.

III. SEVERE ACCIDENT MODELING FOR A VVER-1000 NPP

BAGIRA has recently been upgraded by modeling reactor core degradation phenomena allowing it to model and analyze hypothetical severe accidents at NPPs. In the following section we describe an example of a severe accident analysis that models double-ended cold leg LOCA with simultaneous ECCS's failure at a VVER-1000. For more detailed discussion of the severe accident models see the paper.[7]

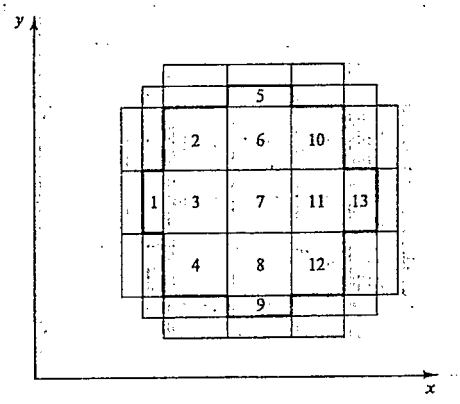

Fig. 19. Reactor vessel nodalization scheme (top view) (numbers indicate number of fuel rod groups).

The reactor vessel contained 259 cells: 37 cells in horizontal cross section (see Fig. 19) and 7 layers in the core axial direction. In the neutron kinetics model all fuel rods was individually modeled, however, for the thermal-hydraulic calculations, all rods in a cell were substituted by an effective fuel rod (leading to 13 effective rods). Each effective fuel rod was characterized by an average clad temperature, which served as a failure criterion.

The list of main events during the accident is given in Table IV.

TABLE IV

Main events during the severe accident process

Event	Time, minutes
Cold leg, double-ended rupture	0.0
Start of vapor-zirconium reaction and hydrogen release	2.5
Zirconium melting starts	8.5
Fuel rod clad failure starts	10.5
Fuel melting starts	53
Destruction of No. 7 fuel rod group	184
Destruction of No. 3, 6, 8, and 11 fuel rod groups	223
Destruction of No. 2, 4, 10, and 12 fuel rod groups	231
Reactor bottom melt-through	380
Reactor cavity bottom complete ablation	~3000

Fig. 20 shows the vertical component of the coolant velocity distribution in the lower part of the reactor core (horizontal cross section) as calculated by the code at time t = 184 minutes, i.e., just before the destruction of the No. 7 fuel rod group. The negative velocity values (shown below the x-y plane in peripheral regions) correspond to coolant velocities in the downcomer. It is important to recognize that the gas velocity distribution in lower parts of the core is non-uniform and essentially asymmetric, even though the initial heat release distribution is symmetric with respect to the core center. The initial symmetry is affected by the location of the loop rupture resulting in an asymmetrical distribution.

The local velocity maximum seen in the middle of the core is caused by the maximum local heat release. The characteristic coolant velocities in the 1st and 13th zones are greater than in the 5th and 9th zones, since the reactor vessel and primary loop junctions are closer to these zones. In fact, zone No. 1 is the closest to the broken loop with the maximum coolant velocity value. The velocity distribution is also affected by the change of flow area caused by the destruction of the fuel rods. From Fig. 20 it is seen that the relative non-uniformity of the velocity distribution reaches 70% in the horizontal cross section.

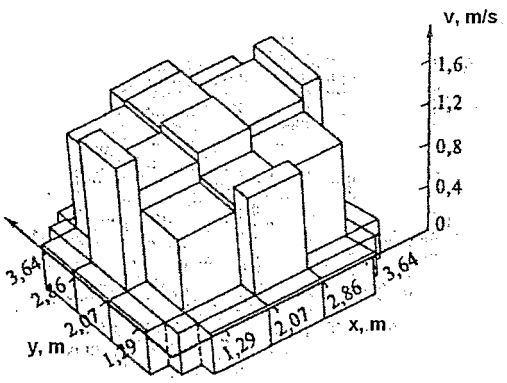

Fig. 20. Coolant (gas) velocity distribution at t = 184 minutes along the lower part of the reactor (horizontal cross section)

Fig. 21 shows the gas temperature distribution in the vertical cross section of the reactor, passing through the center of the core (zones 1, 3, 11, and 13). The plot corresponds to the time t = 380 minutes, just preceding the destruction of the reactor bottom. By this time the middle of the core has no fuel as all the rods have already melted and fell down to the reactor bottom. Note that in the middle of the core gas heating occurs only due to irradiation and turbulent mixing. As a consequence, the gas temperature is less in the central than the peripheral regions, which still have intact fuel rods in place. Fig. 21 also indicates that the gas temperature reaches its maximum in the upper, peripheral part of the core (4th and 5th layers along z). The local gas temperature minimum in the 1st and 13th zones (at the 6th layer along z) is caused by gas flow from the core central regions to the hot legs.

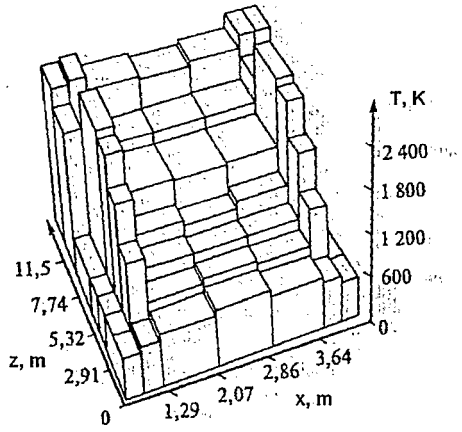

Fig. 21. Coolant temperature distribution in the vertical cross section of reactor, passing through the symmetry axis of the core at t = 380 minutes

It is clear that the gas temperature distribution is strongly non-uniform in the reactor vessel with a relative difference between the central and peripheral zones exceeding more than 100%.

IV. CONCLUSIONS

Based on the results discussed above, BAGIRA is considered an effective tool for comprehensive numerical analysis of complex two-phase flow phenomena in NPP circuits. It is capable of accurately analyzing steady-state, transient, and accident events in different operational regimes. Combined with specifically designed core degradation models, BAGIRA can also be applied for complex severe accident analysis.

One of the most attractive features of the code is its capability to perform multi-dimensional calculations. The mathematical model is based on numerical approximations to exact three-dimensional equations, which is in contrast to many codes using one-dimensional representation of inherently multi-dimensional geometries and associated physical phenomena. In addition, BAGIRA includes effective multi-dimensional models for turbulent heat and mass transfers. Experimental observations as well as calculational experience indicate that multi-dimensional effects may play a significant role in many phenomena affecting the operation safety of NPP.

An effective numerical scheme allows real-time, highly-accurate computations together with multi-dimensional models for the reactor vessels and SG's. This provides a promising perspective for using BAGIRA in power plant simulators. VNIIAES developed full-scope and analytical simulators using BAGIRA for a number of power plants with VVER-1000, VVER-440, and RBMK type designs, which included the Kalinin, Kursk, Smolensk, Chernobyl, and Bilibino NPPs.

NOMENCLATURE

Acronyms:

ECCS – emergency core coolant system;
LOCA – loss-of-coolant accident;
MCP – main coolant pump;
NPP – nuclear power plant;
SG – steam generator.

Physical quantities:

α – phase volumetric fraction;
L – water level [m];
N – relative reactor power [%];
p – pressure [Pa];
t – time [s];
T – temperature [°C, K] ;
v – velocity [m/s];
w – mixture volumetric velocity [m/s];
x, y, z, X, Y, Z – spatial coordinates [m].

REFERENCES

1. A. E. KROSHILIN, V. E. Kroshilin, A. N. Veselovsky, S. D. Kalinichenko, and A. F. Zhivotyagin, "Modeling of Three-Dimensional Time Dependent Two-phase Flow For Full Scope Training Simulators with BAGIRA Thermal-Hydraulic Code," *Proc. of the 1994 Simulation Multiconference*, pp. 494-499, San Diego, California, USA (April 10-14, 1994).

2. A. E. KROSHILIN, V. E. Kroshilin, M. R. Fakory, W. Shire, and P. Kohut, "Analysis of 3-Dimensional Two-Phase Flow for Real-Time Training Simulators with Engineering Analysis Code (BAGIRA)," *Proc. of the 1996 Simulation Multiconference*, pp. 56-62, New Orleans, Louisiana, USA (April 8-11, 1996).

3. S. D. KALINICHENKO, A. E. Kroshilin, V. E. Kroshilin, A. V. Smirnov, and P. Kohut, "Three-Dimensional Thermal-Hydraulic Best Estimate Code BAGIRA: New Verification Results," *Proc. of the 11-th International Topical Meeting on Nuclear Reactor Thermal Hydraulics (NURETH-11)*, Paper 105, Avignon, France (October 2-6, 2005).

4. S. D. KALINICHENKO, P. Kohut, A. E. Kroshilin, V. E. Kroshilin, and A. V. Smirnov, "BAGIRA: A 3-D Thermal Hydraulic Code for Analysis of Complex Two-Phase Flow Phenomena," *Proc. of the 2003 International Congress on Advances in Nuclear Power Plants (ICAPP'03)*, Paper 3352, Cordoba, Spain (May 4-7, 2003).

5. S. D. KALINICHENKO, A. E. Kroshilin, V. E. Kroshilin, A. V. Smirnov, and P. Kohut, "Experimental Verification of the Three-dimensional Thermal-Hydraulic Models in the Best-Estimate Code BAGIRA," *Proc. of the 2004 International Congress on Advances in Nuclear Power Plants (ICAPP'04)*, Paper 4079, Pittsburgh, PA USA (June 13-17, 2004).

6. *Investigation of hydrodynamic and thermal characteristics of VVER-1000 steam generator at N-VNPP Unit 5.* Final report No. 187-0217, OKB GIDROPRESS, Podolsk (1982).

7. A. E. KROSHILIN, V. E. Kroshilin, and R. L. Fuks, "Simulation of Extreme Situations at an NPP with a VVER-1000 Reactor Using the BAGIRA-SAM Package of Computer Codes," *Thermal Engineering*, **48**, *No. 12*, p. 979 (2001).